Hindawi
Scientific Programming
Volume 2021, Article ID 1125573, 7 pages
https://doi.org/10.1155/2021/1125573

Research Article

Artificial Intelligence-Based CT Images in Analysis of Postoperative Recovery of Patients Undergoing Laparoscopic Cholecystectomy under Balanced Anesthesia

Manyun Bai,[1] **Renzhong Guo**,[2] **Qian Zhao**,[1] **and Yufang Li**[1]

[1]*Department of Anesthesiology, The Fourth Hospital of Changsha (Changsha Hospital of Hunan Normal University), Changsha 410006, Hunan, China*
[2]*Department of Otorhinolaryngology-Head and Neck Surgery, Changsha Central Hospital (Changsha Central Hospital Affiliated to University of South China), Changsha 410004, Hunan, China*

Correspondence should be addressed to Yufang Li; 1751030136@xzyz.edu.cn

Received 10 July 2021; Revised 12 August 2021; Accepted 13 August 2021; Published 2 September 2021

Academic Editor: Gustavo Ramirez

To explore whether preoperative processing can promote the recovery of gastrointestinal function after laparoscopic cholecystectomy (LC) surgery, in the study, an artificial intelligence-based algorithm was used to segment the CT images to assist doctors in decision making. The patients were divided into observation group (balanced anesthesia) and control group (general anesthesia) with SPSS. The observation group received balanced anesthesia half a day before the operation. The method of balanced anesthesia was to induce 0.2 mg/kg midazolam, 3 mg/kg propofol, 2 μg/kg remifentanil, 0.2 mg/kg vecuronium, 4~5 mg/(kg·h) propofol, and 9~11 μg/(kg·h) remifentanil continuous intravenous infusion to maintain anesthesia, and it was stopped once the patient defecated; the control group had general anesthesia in the afternoon after the operation, and it was stopped once the patient defecated. The time before the first exhaust and defecation after the surgery as well as the recovery time of bowel sound was recorded, and the degree of abdominal pain, abdominal distension, and gastrointestinal adverse reactions was evaluated at 22 hours, 46 hours, and 70 hours after the surgery. It was found that the accuracy of the artificial intelligence-based segmentation algorithm was 81%. The reconstruction accuracy of multidimensional liver could be observed at any angle, and the reconstruction accuracy was not lower than the resolution of original input CT. The calculation error was less than 9%, and the volume of whole liver, liver segment, preresection liver, and residual liver was less than 9%. The simulation accuracy of virtual liver surgery was not lower than the resolution of original input CT. The time before the first exhaust and defecation was shorter in the observation group versus the control group ($P < 0.05$). The recovery time of bowel sound in the observation group was shorter than that in the control group ($P < 0.05$). There was a significant difference in the scores of abdominal distension between the two groups at 22 h and 46 h after surgery ($P < 0.05$). It suggested that both the observation group and the control group could improve the symptoms of gastrointestinal adverse reactions after surgery. Nevertheless, balanced anesthesia can shorten the time before the first exhaust and defecation after surgery and promote the recovery of postoperative bowel sound. Furthermore, balanced anesthesia can alleviate abdominal distension, abdominal pain, and gastrointestinal adverse reactions, which should be promoted in clinic.

1. Introduction

With the continuous development of the economy, people's living habits have changed, and many people suffer from benign gallbladder diseases [1]. Studies have pointed out that the incidence of gallstones in China is approximately 9.9% to 13% [2], and in the United States, the incidence of gallstones is 7.2%, the incidence of cholecystitis is 2.1% to 4.2%, and the incidence of gallbladder polyp is 4.9% to 5.86% [3]. Usually, benign gallbladder disease does not threaten the life [4]. Studies have shown that the occurrence of gallbladder disease will increase the incidence of cardiovascular disease

and gallbladder cancer, increasing financial burden on the patient's family. Surgery is an effective way to treat benign gallbladder diseases, especially laparoscopic cholecystectomy (LC) [5]. It has been reported that LC can minimize trauma and complications, reduce recovery time, and improve postoperative quality of life. It has little impact on liver and kidney function [6]. The surgical site is mainly the right upper abdomen, and LC surgery does not cause immediate damage to the gastrointestinal tract [7], and the use of stable analgesics affects the recovery of gastrointestinal function after surgery [8]. 27.6% of patients undergoing LC surgery have complications, such as difficulty in defecation and severe intestinal paralysis [9].

Gastrointestinal dysfunction after the surgery affects the patient's quality of life [10], and the recovery of gastrointestinal function is important [11]. Image segmentation is a commonly used method to process medical images [12], and it provides a scientific means for surgeons to locate, guide, and simulate [13]. Although LC has been widely used in clinical practice, the anesthesia effects directly affect the efficiency of the operation and the patient's feeling of satisfaction [14]. In the CT image examination method, the CT image is sent to the EBW workbench and MPR, MIP, MINP, and other postprocessing are carry out at the workstation. Anesthesia can not only affect the immune function but also interfere with the immune function through stress response. In laparoscopic surgery, it is very important to use the appropriate amount of anesthetic because anesthesia may also increase the risk of perioperative accidents. Balanced anesthesia can improve abdominal distension symptoms and gastrointestinal adverse reactions. In this study, an artificial intelligence-based algorithm was used to segment CT images to explore whether postoperative pretreatment can help improve gastrointestinal function after LC surgery, providing a new method for clinical treatment of the gallbladder diseases.

2. Materials and Methods

2.1. Research Subjects. A total of 180 patients in the hospital from February 2017 to December 2020 were selected as the research subjects. They were selected as per the following inclusion criteria: (I) patients who met the diagnosis standard of this disease; (II) patients who had surgical indications and were classified as grades I to III according to the American Society of Anesthesiologists (ASA); (III) aged between 19 and 65 years old; and (IV) patients who had signed an informed consent form. Exclusion criteria were as follows: (I) patients who cannot speak or with audiovisual problems and mental illness; (II) pregnant and lactating patients; (III) patients with hyperthyroidism, immune problems, blood diseases, trauma, fractures, and other diseases that affected gastrointestinal motility; (IV) patients with serious heart, lung, liver, or kidney diseases; and (V) patients with ascites. Criteria for drug withdrawal: (1) serious adverse problems and feelings occurred during treatment; (2) during the experiment, the loss rate of subjects was more than 19%.

Initially, a total of 200 cases were collected, and 20 cases were excluded according to the exclusion criteria. Then, a total of 180 patients were enrolled in this study, including 100 in the gallstone group and 80 in the control group. The gallbladder stone group included 30 cases of simple gallbladder stones, 32 cases of gallbladder stones with acute cholecystitis (including acute episodes of chronic cholecystitis), and 38 cases of gallbladder stones with chronic cholecystitis. This study had been approved by the Medical Ethics Committee of the hospital, and the family members of the patients included in the study had signed the consent form.

2.2. CT Scan. Philips 348-layer spiral CT (Britain) and EBW workshop were used. Due to the small size of the saccular artery, the angiographic contrast agent ioversol (269 mg I/mL) or iodohexanol (412 mg I/mL) was used. The arterial phase scan gap was determined using the contrast agent spontaneous targeting method. The monitoring point was set on the abdominal aorta on the top of the diaphragm, and then the monitoring scan was started. When the observation point threshold reached 149 HU, the scan started, and the scan delay time was 7.3 s. The scan area was from the diaphragm to the iliac crest. The venous phase scan was performed 29 s after the beginning of the arterial phase, and the patient held his breath during the scan (the patient was trained to hold his breath before the scan). A double-barrel automatic high-pressure syringe was used to inject 79–91 mL of contrast through the anterior vein of elbow joint. The injection flow rate was 4.9 mL/s, and 18 mL of normal saline was injected later to flush the contrast.

Scanning parameters were as follows: tube voltage—119 kV, tube current—287 mAs, collimation—135 layers × 0.735 mm, rotation time—0.45 s/*r*, spacing—0.887, matrix—543 × 543, and reconstruction algorithm—standard (A).

2.3. Artificial Intelligence-Based Segmentation Algorithm. The CT images were sent to the EBW workbench for postprocessing, such as MPR, MIP, and MINP. The saccular artery and saccular tube were highlighted first. To find the gallbladder artery, first, it was needed to find the branch of the gallbladder artery, and then the main part of the gallbladder artery was traced. To find the cystic duct, first, it was needed to find the cystic duct in the neck area of the gallbladder, and then the location of common liver ducts was traced. To reconstruct the triangle structure of the gallbladder, first, the direction of cystic duct was determined through the venous phase image, and then the polygonal shape of the gallbladder was reconstructed using MIP and MPR techniques on coronary phase image.

The bile duct segmentation algorithm is operated as follows. (I) The seed point is marked and included into the stack. (II) From the stack, if the difference meets the condition, the mark is put into the stack. If not, return to (II). If these operations have been performed, the program will end. (III) The edge of the initial segmentation result is used as the seed point.

During image processing, convolution is performed on each input pixel. For many problems, the linear expression is far from the expected effects, so the activation function is introduced. $f(x) = 1/l + e{-}x$. The function can be continuously differentiated in the domain. It is easy to calculate and has a wide range of application prospects. The derivative function is expressed as follows: $F'(x) = f(x) * (1{-}f(x))$.

It is assumed that the parameters of the neural network are as follows: x_l^d $(d = 1,2, \ldots, n_d)$ is the input sample; then, x_l^d is the component of each sample, u_{gl} is the weight of x_l^d and the g-th neuron, and C_{lg} is the output; then, the input and output will satisfy the following equation:

$$\frac{dC_{lg}}{dt} = \sum_{i=1}^{n} u_{gl} x_l^d - \Upsilon\left(C_{lg}\right). \tag{1}$$

In the equation, the weighted cumulative sum of $\sum_{i=1}^{n} u_{gl} x_l^d$ input and $\Upsilon(C_{lg})$ is a function to slow down the change speed of C_{lg}, which is simplified as follows:

$$C_{lg} = \sigma\left(\sum_{l=1}^{n} u_{lg} x_l^{qd}\right), \tag{2}$$

where $\sigma(\bullet)$ is a monotonically rising nonlinear function and u_{lg}'s learning meets the law and comes to the following conclusion:

$$\frac{du_{\overline{J}}}{dt} = \alpha C_{lg} x_l^d - \beta\left(C_{lg}\right)\omega_{\overline{S}}. \tag{3}$$

When $C_{lg} \in [0, 1]$, C_{lg} satisfies $C_{lg} = o$, $\beta(C_{lg}) = 0$, $C_{lg} = 1$, and $\beta(C_{lg}) = \alpha$, then equation (4) can be obtained:

$$\begin{cases} \dfrac{d\omega_{ji}}{dt} = \alpha\left(x_i^q - \omega_j\right), & C_{ij} = 1, \\ \dfrac{d\omega_{ji}}{dt} = 0, & C_{ij} = 0. \end{cases} \tag{4}$$

The learned weight can be obtained from (4), u_{gl} is getting closer and closer to the input X_l^k, and the overall result makes the automatic sorting of some irregular inputs and the distribution of weighted values similar to the probability density distribution of input samples.

Convolutional neural network (CNN) is a common deep learning algorithm. The process is as follows: (I) it is triggered by the human visual system; (II) it constantly changes; and (III) it is formed in a multilayer neural network suitable for image processing and recognition. Figure 1 shows the structure of a classic CNN composed of a convolutional neural layer and a normalization layer.

2.4. Anesthesia and Treatment. 0.4 mg of atropine and 0.2 g of phenobarbital were injected intramuscularly 40 min before surgery. In the observation group, midazolam 0.2 mg/kg, propofol 3 mg/kg, remifentanil 2 μg/kg, and vecuronium 0.2 mg/kg were administered. During the surgery, propofol 4 ~ 5 mg/(kg·h) and remifentanil 9 ~ 11 μg/(kg·h) were injected intravenously, and vecuronium bromide was administered according to the specific situation. In the control group, fentanyl 6 μg/kg, midazolam 0.2 mg/kg, disoprofol 3 mg/kg, vecuronium 0.2 mg/kg, and 0.7%~2.5% isoflurane were used for anesthesia. The rest was the same as the observation group. Both groups discontinued the drug at the end of the surgery. The operation time was 40 to 80 minutes.

In the observation group, preoperative balanced anesthesia was adopted, and the patient took the supine position. 80% alcohol was used to disinfect hands and needles before surgery. If the patient had not defecated for 4 days after the surgery, the course of treatment was terminated.

In the control group, general anesthesia was adopted, and the patient took a supine position. Before the operation, alcohol was used to disinfect the hands with 80% alcohol. The needle hole was pressed with a sterile cotton swab or cotton ball to prevent bleeding. If the patient had not defecated for 4 days after the surgery, the course of treatment was terminated.

2.5. Observation Indicators. In terms of the image segmentation effects, the image segmentation index was used. On the test set, the prediction results obtained by the segmentation algorithm were compared with the actual results. The correct pixel resolution was called "positive," and the wrong pixel resolution was called "negative." A two-dimensional matrix was used to calculate. Table 1 shows the evaluation index matrix and the image segmentation entanglement matrix. TP is true positive, FP is false positive, FN is false negative, and TN is true negative (Table 1).

According to clinical signs, symptoms, and CT scan results, gallstone patients were divided into simple gallstone group, acute jaundice gallstone group (including acute attack of chronic jaundice), chronic jaundice gallstone group, and chronic cholera group. (I) Simple gallbladder stone group: CT results showed gallbladder stones, and the surface fat around the gallbladder was clean. (II) Gallbladder dissolution with acute cholecystitis group (including acute attack of chronic cholecystitis): CT results showed that the gallbladder volume increased and the volume of fat around the gallbladder increased. (III) Gallbladder stones with chronic cholecystitis group: CT results showed that gallbladder stones were accompanied by gallbladder wall thickening (wall thickening) and the fat space around the gallbladder was clear.

2.6. Statistical Analysis. SPSS 16 was used to process the data. The continuous variables were expressed as mean ± standard deviation, and categorical variables were expressed by percentages. The mean comparison of two pairs of continuous variable data adopted t-test, the mean of continuous variable data used analysis of variance, and the mean comparison of two groups and more than two groups adopted the chi-square test. $P < 0.05$ was the threshold for significance.

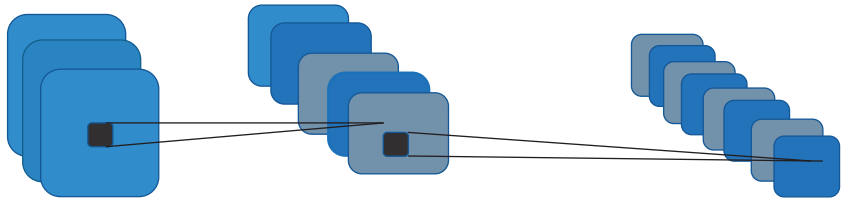

Figure 1: CNN model.

Table 1: Confusion matrix.

		Standard set		
		T (true)	F (false)	In total
Test sample	P (judgment exists)	TP (predicted result is positive, and the actual result is positive)	FP (predicted result is positive, and the actual result is negative)	P (the predicted result is positive)
	N (judgment does not exist)	FN (predicted result is negative, and the actual result is positive)	TN (predicted result is negative, and the actual result is negative)	N (the judgment is negative)
	In total	T (true)	F (false)	TP + FN + FP + TN

3. Results

3.1. Basic Information of the Patients. After *t*-test and chi-square test, there was no statistically significant difference in age, gender, and contrast agents between the gallbladder stone group and control group (Table 2).

3.2. Image Segmentation Effect Based on Artificial Intelligence. The main technical indicators are as follows: the automatic segmentation accuracy is greater than 79%; the reconstruction of the liver allows observation in multiple dimensions, and the reconstruction accuracy is not lower than the original CT resolution; the calculation error is less than 9%; and the volume of the whole liver, liver segment, the removed liver, and residual liver is less than 9%. Conclusion: the simulation accuracy of virtual liver surgery (conventional liver resection and irregular liver resection) was not lower than the original input CT resolution. Figure 2 shows the segmentation results of the target area in the CT image.

3.3. Evaluation Indicators of Treatment Effects. The first postoperative exhaust and defecation time was compared with that of the control group, and there was statistically significant difference ($P < 0.05$), as shown in Figures 3 and 4, suggesting that both of the two methods can reduce the time before the first exhaust and defecation after LC, but the balanced anesthesia observation group showed better therapeutic effects with shorter time before the first exhaust and defecation after LC.

The recovery time of bowel sound in the observation group was shorter than that in the control group, and the difference was statistically significant ($P < 0.05$), suggesting that the balanced anesthesia observation group showed better therapeutic effects with shorter recovery time of bowel sound. As shown in Figure 5, balanced anesthesia can reduce the recovery time of bowel sound after surgery. The patients can accept acupuncture and moxibustion in advance to dredge the meridians and strengthen the gastrointestinal movement, so as to enhance the therapeutic effects. The recovery time of tinnitus in the observation group was 14.38 ± 5.5. The recovery time of bowel sound in the observation group was 12.87 ± 4.67.

Figure 6 shows the postoperative abdominal distension in the observation group and the control group. It was noted that there was statistically significant difference between the two groups ($P < 0.05$). It was proved that preoperative balanced anesthesia can alleviate the degree of abdominal distension after surgery. There was also a statistically significant difference in the abdominal pain after LC between the two groups, as shown in Figure 7. It suggested that balance anesthesia can alleviate the degree of abdominal pain. There was no statistically significant difference between the two groups in the improvement of abdominal pain after LC, which may be related to the small sample size.

Figure 8 shows the gastrointestinal function after the LC surgery in the observation group and the control group. It was noted that abdominal distension scores of the two groups were statistically significant at 22 h and 46 h after surgery ($P < 0.05$), while there was no statistically significant difference between the two groups at 46 h and 70 h after the operation ($P > 0.05$). There was statistically significant difference in abdominal distension after the LC surgery between the two groups ($P < 0.05$). Hence, it was inferred that both the observation group and the control group could improve the symptoms of gastrointestinal reactions after surgery, and both groups alleviated the symptoms of gastrointestinal reactions at 46 h, but the observation group had better results at 22 h after surgery. The gastrointestinal reaction of the two groups was relieved at 46 hours after operation, which may be related to the promotion of gastrointestinal motility after eating.

4. Discussion

In recent years, artificial intelligence technology has broad application prospects in medical field [15]. The segmentation effects are affected by the specific imaging mode, the body

Table 2: Basic information of patients.

	Gallbladder stone group (%)	Control group	P value
Age	55 ± 2.4	50 ± 12	$P > 0.05$
Sex: Male	58.4%	58.3%	$P > 0.05$
Female	41.5%	41.2%	
Contrast agent			$P > 0.05$
Iopamidol (Germany) (363 mgI/mL)	52.9%	55.7%	

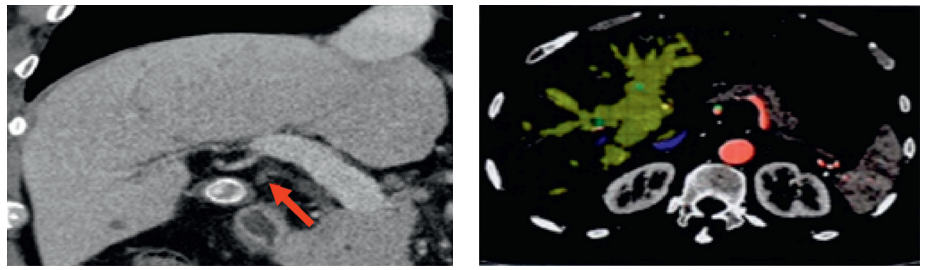

(a) (b)

Figure 2: Comparison of patients before and after CT image segmentation. (a) CT image of the bile duct. (b) Segmentation of the target area in the CT image.

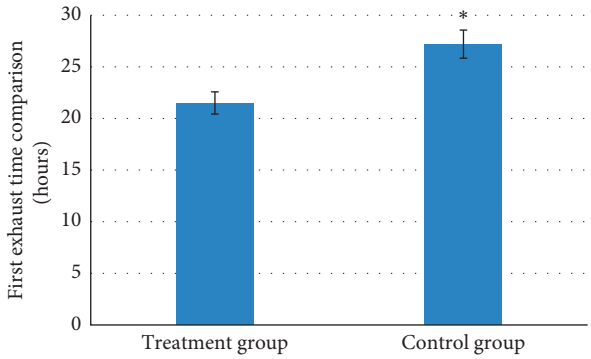

Figure 3: Comparison of the first exhaust time between the two groups. *A significant difference between the two groups, $P < 0.05$.

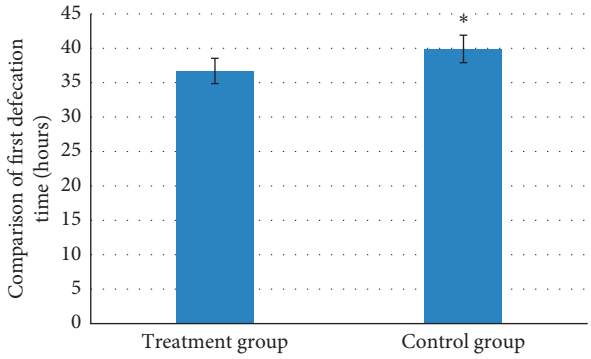

Figure 4: Comparison of the first defecation time between the two groups. *A significant difference between the two groups, $P < 0.05$.

area, and the ability of the segmentation algorithm, and some algorithms that have good results in ordinary images cannot achieve the same effects on medical images [16].

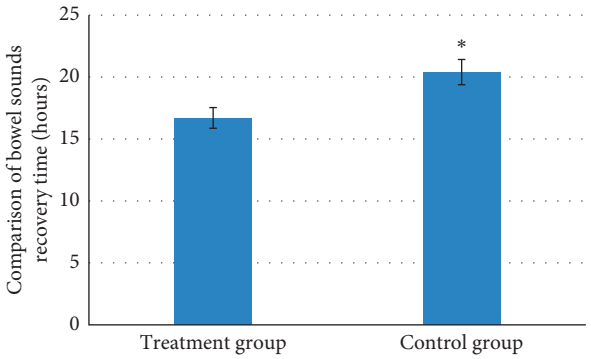

Figure 5: Comparison of the recovery time of bowel sound between the two groups. *A significant difference between the two groups, $P < 0.05$.

Therefore, a medical image segmentation algorithm is required, and it is designed according to the specific imaging mode, body area, and application scene. The particularity of medical image imaging modes has brought problems such as medical artifacts and noise, affecting medical image segmentation effects to general image segmentation. To enhance the adaptability and performance of the threshold segmentation algorithm in the medical field [17], it needs to be optimized to reduce the artifacts and noise. In China, conventional CT plain scans for LC surgery have been recognized and accepted by clinicians, but the importance of CT enhanced scans in LC surgery has not been fully realized. This requires further research by imaging doctors [18].

LC has become the first choice for the treatment of common gallbladder diseases, especially gallbladder stones and cholecystitis. However, the incidence of gallbladder artery hemorrhage and bile duct injury arising from LC is not lower than that of open cholecystectomy. Inflammatory adhesions of the gallbladder triangle lead to unclear display

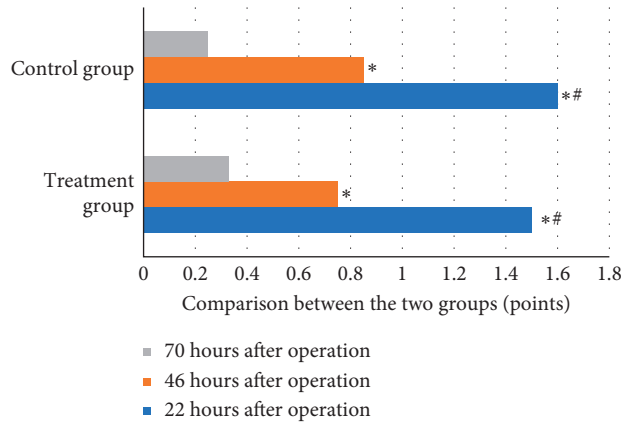

Figure 6: Comparison of abdominal distension between the two groups. Note: compared with 70 hours after operation, $^{*}P < 0.05$; compared with 46 hours after operation, $^{\#}P < 0.05$.

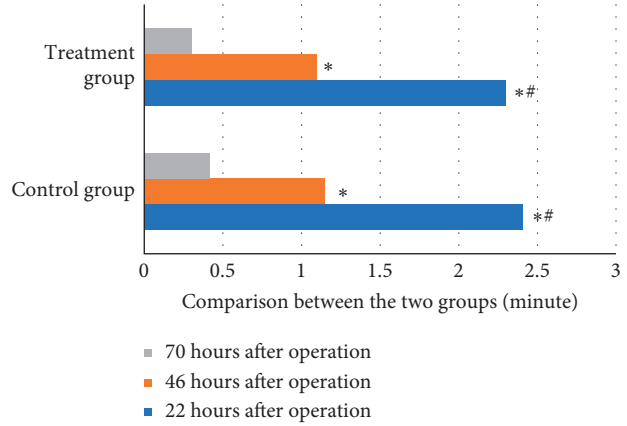

Figure 7: Comparison of abdominal pain between the two groups. Note: compared with 70 hours after operation, $^{*}P < 0.05$; compared with 46 hours after operation, $^{\#}P < 0.05$.

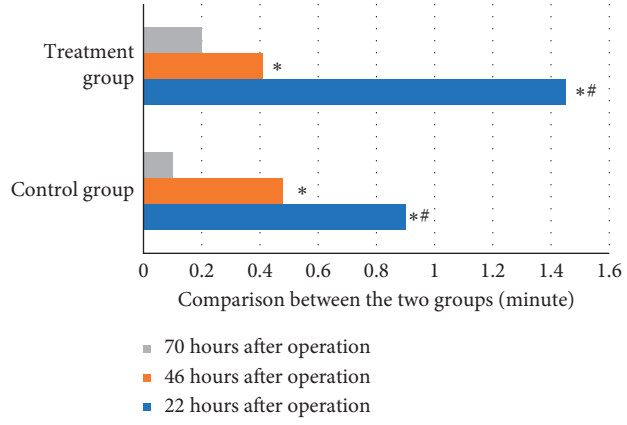

Figure 8: Gastrointestinal reaction comparison between the two groups. Note: compared with 70 hours after operation, $^{*}P < 0.05$; compared with 46 hours after operation, $^{\#}P < 0.05$.

of part of the anatomical structure, which can be attributed to the variations in the anatomical structure of the gallbladder triangle and small laparoscopic field of view [19]. With the continuous improvement of doctors' surgical skills, many open surgeries have now been replaced by endovascular surgeries. There are high requirements on anesthesia effects for laparoscopic surgery, and due to the short operation time, better controllability is required. Remifentanil is a short-acting synthetic opioid, characterized by fast onset, short action time, repeated use without accumulation, and strong analgesic effects. Propofol is a short-acting intravenous anesthetic, which can be used in combination with remifentanil to make up for the weak sedative effects of opioids [20]. Currently, remifentanil combined with propofol intravenous maintenance anesthesia is the best choice for the anesthesia for LC surgery [21]. The convolutional neural network in this research has the advantages of simple calculation, clear image, and wide application prospect [22]. Balanced anesthesia can create better surgical conditions than general anesthesia, which not only fully ensures the safety of patients during operation but also ensures the postoperative recovery of patients. Balanced anesthesia could shorten the first exhaust and defecation time and promote the recovery of postoperative intestinal sound. It can reduce abdominal distension, abdominal pain, and gastrointestinal adverse reactions.

5. Conclusion

In the study, it was found that balanced anesthesia treatment can shorten the time before the first postoperative exhaust and defecation and reduce the recovery time of postoperative bowel sounds, and compared to other methods, there are obvious differences ($P < 0.05$). Additionally, it can alleviate abdominal distension, abdominal pain symptoms, and gastrointestinal adverse reactions. After the comparison of the safety and effectiveness between the observation group and the control group, it was concluded that balanced anesthesia is feasible and worthy of clinical promotion. However, there are also many problems in the study. First, in practice, despite the good image quality of the bile duct, due to incomplete data, this study cannot measure the BMI of all patients. The artificial intelligence algorithm used in this article has not been compared and analyzed with other advanced algorithms, and it cannot prove the excellent performance of the algorithm used in this article. Further, the sample size is too small, and in the follow-up, an expanded sample size is needed to strengthen the findings of the study.

Data Availability

The data used to support the findings of this study are available from the corresponding author upon request.

Conflicts of Interest

The authors declare that they have no conflicts of interest.

References

[1] L. L. Fan, B. H. Chen, and Z. J. Dai, "The relation between gallstone disease and cardiovascular disease," *Scientific Reports*, vol. 7, no. 1, Article ID 15104, 2017.

[2] A. Venara, M. Neunlist, K. Slim et al., "Postoperative ileus: pathophysiology, incidence, and prevention," *Journal of Visceral Surgery*, vol. 153, no. 6, pp. 439–446, 2016.

[3] M. Jenks, M. Taylor, and J. Shore, "Cost-utility analysis of the insufflation of warmed humidified carbon dioxide during open and laparoscopic colorectal surgery," *Expert Review of Pharmacoeconomics & Outcomes Research*, vol. 17, no. 1, pp. 99–107, 2017.

[4] D. Balayssac, B. Pereira, J.-E. Bazin, B. Le Roy, D. Pezet, and J. Gagnière, "Warmed and humidified carbon dioxide for abdominal laparoscopic surgery: meta-analysis of the current literature," *Surgical Endoscopy*, vol. 31, no. 1, pp. 1–12, 2017.

[5] R. A. Travagli and L. Anselmi, "Vagal neurocircuitry and its influence on gastric motility," *Nature Reviews Gastroenterology & Hepatology*, vol. 13, no. 7, pp. 389–401, 2016.

[6] T. Oláh, T. Poór, K. Somodi, G. Baradnay, and T. Halász, "The role of laparoscopy in the surgical treatment of colorectal cancer. Initial results," *Magyar Onkologia*, vol. 47, no. 4, pp. 381–383, 2003.

[7] P. Maruna, R. Gürlich, and R. Frasko, "Pathophysiology of postoperative dysfunctions of the intestinal motility. A review," *Rozhl Chir*, vol. 84, no. 7, pp. 356–362, 2005.

[8] C. E. Murry, R. B. Jennings, and K. A. Reimer, "Preconditioning with ischemia: a delay of lethal cell injury in ischemic myocardium," *Circulation*, vol. 74, no. 5, pp. 1124–1136, 1986.

[9] N. Kotani, H. Hashimoto, Y. Sato et al., "Preoperative intradermal acupuncture reduces postoperative pain, nausea and vomiting, analgesic requirement, and sympathoadrenal responses," *Anesthesiology*, vol. 95, no. 2, pp. 349–356, 2001.

[10] J. M. Polak, A. G. Pearse, and C. M. Heath, "Complete identification of endocrine cells in the gastrointestinal tract using semithin-thin sections to identify motilin cells in human and animal intestine," *Gut*, vol. 16, no. 3, pp. 225–229, 1975.

[11] W. He, X.-Y. Wang, H. Shi et al., "Cutaneous neurogenic inflammation in the sensitized acupoints induced by gastric mucosal injury in rats," *BMC Complementary and Alternative Medicine*, vol. 17, no. 1, p. 141, 2017.

[12] T. Li, W. Gao, and Z.-R. Rao, "Noxious somatic stimulation-induced expression of Fos-like immunoreactivity in catecholaminergic neurons with habenular nucleus projection in the medullary visceral zone of rat," *Brain Research*, vol. 783, no. 1, pp. 51–56, 1998.

[13] R. Wang, Y. Zhou, C. Zhao, and H. Wu, "A hybrid flower pollination algorithm based modified randomized location for multi-threshold medical image segmentation," *Bio-Medical Materials and Engineering*, vol. 26, no. 1, pp. S1345–S1351, 2015.

[14] L. Li, L. Sun, J. Guo, J. Qi, B. Xu, and S. Li, "Modified discrete grey wolf optimizer algorithm for multilevel image thresholding," *Computational Intelligence and Neuroscience*, vol. 2017, Article ID 3295769, 16 pages, 2017.

[15] S. Guo, R. Chen, H. Li, T. Zhang, and Y. Liu, "Identify severity bug report with distribution imbalance by cr-smote and elm," *International Journal of Software Engineering and Knowledge Engineering*, vol. 29, no. 2, pp. 139–175, 2019.

[16] J. Rebelo, K. Fernandes, and J. S. Cardoso, "Quality-based regularization for iterative deep image segmentation," in *Proceedings of the 2019 41st Annual International Conference of the IEEE Engineering in Medicine and Biology Society (EMBC)*, pp. 6734–6737, Berlin, Germany, July 2019.

[17] Y. Kong, J. Wu, G. Yang et al., "Iterative spatial fuzzy clustering for 3D brain magnetic resonance image supervoxel segmentation," *Journal of Neuroscience Methods*, vol. 311, pp. 17–27, 2019.

[18] P. Swierczynski, B. W. Papież, J. A. Schnabel, and C. Macdonald, "A level-set approach to joint image segmentation and registration with application to CT lung imaging," *Computerized Medical Imaging and Graphics*, vol. 65, pp. 58–68, 2018.

[19] S. S. Kim and T. R. Donahue, "Laparoscopic cholecystectomy," *Journal of the American Medical Association*, vol. 319, no. 17, p. 1834, 2018.

[20] S. Park, S.-L. Choi, F. S. Nahm, J.-H. Ryu, and S.-H. Do, "Dexmedetomidine-remifentanil vs propofol-remifentanil for monitored anesthesia care during hysteroscopy," *Medicine (Baltimore)*, vol. 99, no. 43, Article ID e22712, 2020.

[21] M. Khened, V. A. Kollerathu, and G. Krishnamurthi, "Fully convolutional multi-scale residual DenseNets for cardiac segmentation and automated cardiac diagnosis using ensemble of classifiers," *Medical Image Analysis*, vol. 51, pp. 21–45, 2019.

[22] Y. Chen, S. Hu, H. Mao, W. Deng, and X. Gao, "Application of the best evacuation model of deep learning in the design of public structures," *Image and Vision Computing*, vol. 102, Article ID 103975, 2020.